

## Article

# Experimental Study on CO<sub>2</sub> Geochemical Reaction Characteristics in Marine Weakly Consolidated Sandstone Saline Aquifers

Mingying Xie<sup>1</sup>, Zhiyong Tu<sup>1</sup>, Xiaona Sun<sup>1</sup>, Zhenghe Yan<sup>1</sup>, Shasha Feng<sup>1</sup>, Deng Zhang<sup>2</sup>, Fuyang Li<sup>2</sup> and Liang Zhang<sup>2,3,\*</sup> 

<sup>1</sup> Shenzhen Branch of CNOOC China Limited, Shenzhen 518000, China

<sup>2</sup> School of Petroleum Engineering, China University of Petroleum (East China), Qingdao 266580, China

<sup>3</sup> Key Laboratory of Unconventional Oil & Gas Development, China University of Petroleum (East China), Ministry of Education, Qingdao 266580, China

\* Correspondence: zhlypc@upc.edu.cn

**Abstract:** Geological storage is one of the most important measures to reduce carbon emissions. The newly developed oilfield A in the Pearl River Mouth Basin of the South China Sea is associated with a large amount of CO<sub>2</sub> with a purity of up to 95%. Two weakly consolidated sandstone saline aquifers located above the oil reservoir can be used for CO<sub>2</sub> storage, but the CO<sub>2</sub> geochemical reaction characteristics in the aquifers should be investigated clearly, which may cause significant damage to the physical properties of the reservoirs and caprocks of the aquifers. In this paper, static CO<sub>2</sub> geochemical reaction experiments and rock thin section identifications were carried out using drill cuttings and sidewall cores, respectively. A numerical simulation was conducted according to the reactor conditions to explore the equilibrium state of the CO<sub>2</sub> geochemical reaction. Through these studies, the characteristics of the geochemical reaction, its impact on the physical properties of the formation, and the CO<sub>2</sub> storage potential by mineral trapping in the target aquifers were revealed. The results show that the two saline aquifers have similar physical properties. The reservoirs are mostly made up of fine-to-medium-grained sandstones as quartz arenite with a considerable amount of feldspar, which can provide favorable pore space for CO<sub>2</sub> storage, while the caprocks are fine-grained felsic sedimentary rocks that can have a good sealing effect. However, both the reservoirs and caprocks contain a certain amount of carbonate and clay minerals. Mineral dissolution dominates in the CO<sub>2</sub> geochemical reaction process, and more Ca<sup>2+</sup> and Mg<sup>2+</sup> is released into the formation water. The theoretical maximum CO<sub>2</sub> mineral trapping capacity in the aquifers is 0.023–0.0538 mol/100 g rock, but due to the dynamic equilibrium of the geochemical reaction, the amount of mineralized CO<sub>2</sub> in most of the rock samples is negative, and the average utilization factor is only –55.43%. As a result, the contribution of mineral trapping to the CO<sub>2</sub> storage capacity takes –0.32%, which can be ignored. In the future, it is necessary to conduct detailed research to reveal the effect of a CO<sub>2</sub> geochemical reaction on storage safety, especially in offshore weakly consolidated sandstone saline aquifers, which could be important sites for large-scale CO<sub>2</sub> storage in China.

**Keywords:** saline aquifer; mineral trapping; dissolution effect; geochemical reaction; CO<sub>2</sub> storage capacity



**Citation:** Xie, M.; Tu, Z.; Sun, X.; Yan, Z.; Feng, S.; Zhang, D.; Li, F.; Zhang, L. Experimental Study on CO<sub>2</sub> Geochemical Reaction Characteristics in Marine Weakly Consolidated Sandstone Saline Aquifers. *Processes* **2023**, *11*, 3345. <https://doi.org/10.3390/pr11123345>

Academic Editor: Carlos Sierra Fernández

Received: 19 October 2023

Revised: 28 November 2023

Accepted: 29 November 2023

Published: 30 November 2023



**Copyright:** © 2023 by the authors. Licensee MDPI, Basel, Switzerland. This article is an open access article distributed under the terms and conditions of the Creative Commons Attribution (CC BY) license (<https://creativecommons.org/licenses/by/4.0/>).

## 1. Introduction

CO<sub>2</sub> capture, utilization, and storage (CCUS) are important technical measures to reduce carbon emissions [1,2]. CO<sub>2</sub> discharged from large-scale gas sources during the use of fossil fuels can be captured using chemical absorption, physical adsorption, or membrane separation methods. Purified CO<sub>2</sub> can be used as an industrial product for chemical conversion, desalination, and enhanced oil/gas recovery (EOR/EGR) [3]. The amount of CO<sub>2</sub> used in industrial activities is relatively small. CO<sub>2</sub> injection underground

can achieve large-scale geological storage for permanent disposal. Oil and gas reservoirs, saline aquifers, and deep coal beds can be used as geological structures for CO<sub>2</sub> storage. The injected CO<sub>2</sub> can be sequestered in geological structures mainly by structural trapping, dissolution trapping, residual gas trapping, and mineral trapping. In coalbed and shale formations, the adsorption trapping mechanism will also take effect [4–6]. Among these CO<sub>2</sub> trapping mechanisms, structural trapping is the most important, which dominates in the injection and the long-term storage process, but it heavily depends on the sealing properties of caprock. Relatively, mineral trapping is the safest mechanism that can convert CO<sub>2</sub> into stable solid carbonate minerals [7,8]. We are mostly concerned with the safety of CO<sub>2</sub> geological storage. The failure of trapping mechanisms will induce a CO<sub>2</sub> leakage risk. CO<sub>2</sub> injection can cause formation deformation, caprock fracturing, fault opening, formation erosion, and wellbore corrosion. When the failure condition is reached, CO<sub>2</sub> leakage channels will be generated in the geological structure, and then the risk of CO<sub>2</sub> leakage occurs. Actually, CO<sub>2</sub> storage in geological structures is a thermal–hydrological–mechanical–chemical (THMC) coupling process. The CO<sub>2</sub> leakage risk evaluation should consider more coupled factors, such as the effect of CO<sub>2</sub> geochemical reactions on structural trapping [9–11].

Mineral trapping of CO<sub>2</sub> is mainly achieved through a CO<sub>2</sub> geochemical reaction. Many studies have been carried out to reveal the CO<sub>2</sub> geochemical reaction characteristics and mineral storage capacities under different reservoir conditions [12–15]. The numerical simulation results of Zhang (2011) indicated that a CO<sub>2</sub> geochemical reaction in the clean sandstone aquifer (the main rock mineral is quartz with a small amount of calcite and feldspar) can only contribute less than 2% to CO<sub>2</sub> storage potential. When the saline aquifer lithology is sandstone or carbonate rock containing a large amount of soluble minerals such as calcite, clay, and feldspar, the dissolution/precipitation reaction of rock minerals has an important impact on CO<sub>2</sub> storage, and the contribution of a geochemical reaction to CO<sub>2</sub> storage is determined by the specific interaction process and time between CO<sub>2</sub>, formation water, and rock minerals, which can reach up to 4–23% [12]. In recent years, the advantages of CO<sub>2</sub> storage in basalt reservoirs have attracted more and more attention [13–15]. This kind of reservoir contains a large amount of carbon fixation minerals that can release bivalent cations Ca, Mg, and Fe to react with CO<sub>2</sub>. All CO<sub>2</sub> can be converted into carbonate minerals in a short period, which can reduce the dependence of CO<sub>2</sub> trapping on traditional caprock sealing properties. Injecting CO<sub>2</sub> into basalt reservoirs for storage is an important development direction for mineral trapping. Basalts are widely distributed in the United States, India, Iceland, and other countries [16,17]. Terrestrial basalts in China are mainly distributed in the basin margin, which can provide a huge potential for CO<sub>2</sub> mineralization and storage and have broad application prospects [14]. Based on the current published studies, it can be concluded that different geological structures have different CO<sub>2</sub> geochemical reaction characteristics and mineral storage capacities depending on the specific geological conditions. Geochemical reaction analysis and potential evaluation is an important research direction for a new structure for CO<sub>2</sub> storage.

Compared with other structures, saline aquifers are the most promising site for large-scale CO<sub>2</sub> storage projects because of their wide distribution and large storage capacity [18–21]. Offshore saline aquifers are often selected to dispose of the associated CO<sub>2</sub> in the offshore oil and gas fields, such as Sleipner, Snohvit, and Gorgon projects, which have the unique advantages of being close to the CO<sub>2</sub> gas source and far from densely populated places [22–25]. In China, CO<sub>2</sub> geological storage is preferentially carried out in oil reservoirs, which can obtain additional income from EOR. Only two small-scale pilot experiments of CO<sub>2</sub> storage in saline aquifers have been carried out, in the Ordos basin and Junggar area, respectively [26,27]. In recent years, China National Offshore Oil Corporation (CNOOC) has been planning China's first CO<sub>2</sub> storage project in an offshore saline aquifer. The CO<sub>2</sub> comes from the associated gas in the newly developed oil field A in the Pearl River Mouth Basin in the eastern South China Sea. CO<sub>2</sub> will be purified on a platform and injected into the nearby saline aquifers for storage. Two aquifers are available. Due to the

high content of carbonate and clay minerals, and the weak cementation of sandstone, the CO<sub>2</sub> geochemical reaction may have a significant effect on the aquifer's physical properties and further affect the CO<sub>2</sub> storage safety, which needs to be investigated as soon as possible.

In this study, typical drill cuttings and sidewall cores were sampled at different depths from the reservoirs and caprocks of the two aquifers. Drill cuttings were used for static CO<sub>2</sub> geochemical reaction experiments to obtain the geochemical reaction pathway based on the change in rock mineral and formation water compositions. Complete sidewall cores were used for rock thin section identification to observe the CO<sub>2</sub> corrosion to rock pore throat. Numerical simulation was applied to explore the equilibrium state of the CO<sub>2</sub> geochemical reaction. Through these studies, the characteristics of the geochemical reaction, its impact on the physical properties of the formation, and the CO<sub>2</sub> storage potential by mineral trapping in the target aquifers were revealed. Finally, the impact of the geochemical reaction on CO<sub>2</sub> storage safety was discussed.

## 2. Geological Setting

China's eastern coastline is 32,600 km long, inhabiting 40% of the Chinese population and responsible for 60% of gross domestic product (GDP). A large number of CO<sub>2</sub> emission sources such as thermal power plants, steel plants, and chemical plants have been constructed. There are eight big basins distributed from north to south along the eastern coast [28]. A lot of offshore oil and gas fields are located there. Some oil and gas fields in the basins of the South China Sea are associated with a great amount of CO<sub>2</sub>. The CO<sub>2</sub> content in natural gas can be up to 10–65% in DF1-1 and YC13-1 gas fields [29,30]. The captured CO<sub>2</sub> does not have the technical conditions or time window for EOR or being reinjected back to the original reservoirs. To dispose of the associated CO<sub>2</sub>, the offshore saline aquifers near the oil and gas fields are undoubtedly one of the best storage sites.

In the designed offshore CO<sub>2</sub> storage project, the CO<sub>2</sub> is from the gas cap of oilfield A located in the Pearl River Mouth Basin of the South China Sea. The CO<sub>2</sub> content is up to 95%, and it is further purified and injected into the nearby saline aquifers for storage. The peak injection rate of CO<sub>2</sub> is about 300,000 tons/a, and the cumulative CO<sub>2</sub> injection will exceed 1.5 million tons within a 20-year project period. There are two saline aquifers above the oil reservoir. Aquifer Y is buried at a depth of 800–900 m, and the reservoir temperature and pressure are 52.4 °C and 8.39 MPa, respectively, while aquifer H is buried at a deeper depth of 1100–1200 m, and the reservoir temperature and pressure are 66.9 °C and 11.64 MPa, respectively. The reservoirs have excellent porosity and permeability for CO<sub>2</sub> injection, seepage, and storage. These two aquifers are all anticline structures, and the structural trapping mechanism will play an important role. Stably distributed mudstone and mud–sand interlayers with a large thickness can be good caprocks to prevent the CO<sub>2</sub> in the reservoirs from escaping. In addition, saline aquifers Y and H are of moderate size and have a large potential to store all the CO<sub>2</sub>. However, it should be noted that the aquifers are marine weakly consolidated sandstone reservoirs. Due to the shallow burial depth and poor compaction degree, the rock mechanical strength of the aquifers is relatively low. The CO<sub>2</sub> geochemical reaction may have a great impact on the aquifer's physical properties [31–33]. It can not only convert part of CO<sub>2</sub> into carbonate minerals to achieve permanent trapping but also change the porosity, permeability, and mechanical properties of the reservoir and caprock, which may greatly impact the safety of structural storage and other mechanisms [34–37].

## 3. Methodology

### 3.1. Preparation of Samples

The flowchart of the methodology of this study is shown in Figure 1. Three parts are involved, including sample preparation, laboratory experiment, and numerical simulation. To carry out the laboratory experiment, the drill cuttings, sidewall cores, formation water, and CO<sub>2</sub> gas were prepared first.

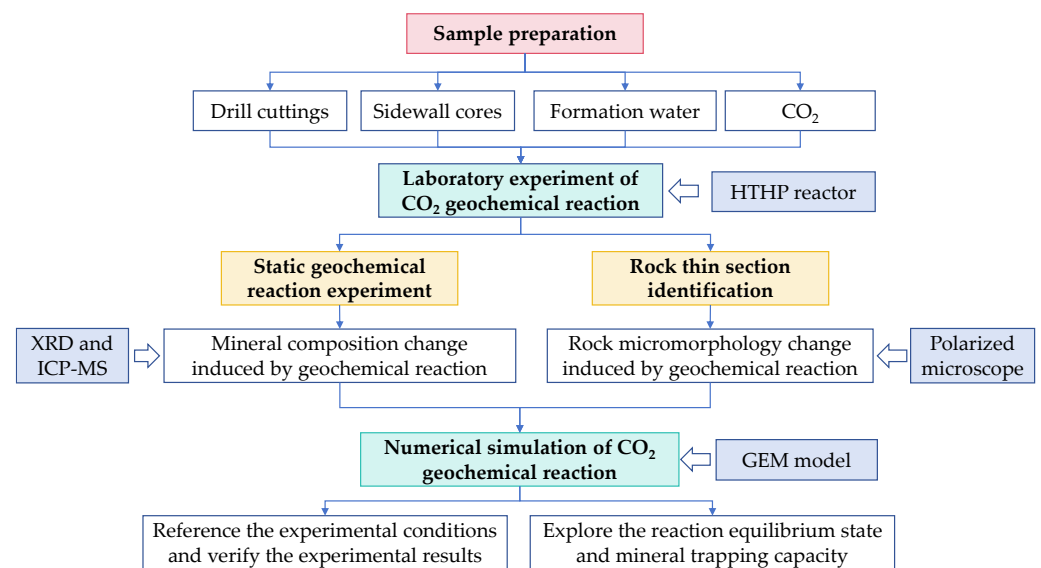


**Figure 1.** Flowchart of based on aims of study and methods utilized in the present study.

- (1) Drill cuttings: The drill cuttings in the typical exploration well located at the top of the anticline drilled through aquifers Y and H were used for static CO<sub>2</sub> geochemical reaction experiments. Ten typical samples at different depths were selected. Five samples are from aquifer Y, while the other five samples are from aquifer H. There are 2 caprock samples and 3 reservoir samples for each aquifer. The sample number represents the sampling depth of cuttings from shallow to deep, as shown in Table 1.

**Table 1.** Rock samples used for the CO<sub>2</sub> geochemical reaction experiments.

Aquifers	Formations	Drill Cuttings		Sidewall Cores	
		No.	Description	No.	Description
Aquifer Y	Caprock	1	Upper caprock	1	Upper caprock
		/	/	2	Middle caprock
		2	Lower caprock	3	Lower caprock
	Reservoir	3	Upper, poor physical properties	4	Upper, poor physical properties
		4	Middle, medium physical properties	5	Middle, good physical properties
		5	Lower, good physical properties	6	Lower, medium physical properties
Aquifer H	Caprock	6	Upper caprock	7	Upper caprock
		/	/	8	Middle caprock
		7	Lower caprock	9	Lower caprock
	Reservoir	8	Upper, good physical properties	10	Upper, good physical properties
		9	Middle, mudstone interlayer	11	Middle, poor physical properties
		10	Lower, medium physical properties	12	Lower, medium physical properties

- (2) Sidewall cores: The complete sidewall cores sampled from an exploration well in a nearby block were used for thin section identification before and after the CO<sub>2</sub> geochemical reaction. The nearby block has the same sedimentary environment and reservoir physical properties as aquifers Y and H. Twelve typical samples at different depths were selected, of which six samples stand for aquifer Y and the other six samples stand for aquifer H. There are 3 caprock samples and 3 reservoir samples for

each aquifer. The sample number also represents the sampling depth of the sidewall cores from shallow to deep and corresponds to the depth of drill cuttings one by one, as shown in Table 1.

- (3) Formation water: The real formation waters taken from the aquifers Y and H were used for the CO<sub>2</sub> geochemical reaction experiment, with a salinity of 37,806 mg/L and 36,991 mg/L, respectively, and their main ion compositions are similar, as shown in Table 2.

**Table 2.** Composition of formation water used for CO<sub>2</sub> geochemical reaction experiments.

Ion Contents, mg/L	Aquifer Y	Aquifer H
K <sup>+</sup>	1455	1078
Na <sup>+</sup>	12,807	12,799
Ca <sup>2+</sup>	494	512
Mg <sup>2+</sup>	214	192
Fe <sup>2+</sup>	0.31	0.14
Fe <sup>3+</sup>	0.65	0.57
Al <sup>3+</sup>	1.07	3.88
Ba <sup>2+</sup>	1.39	3.57
Cl <sup>-</sup>	22,163	21,670
SO <sub>4</sub> <sup>2-</sup>	289	198
HCO <sub>3</sub> <sup>-</sup>	338	457
CO <sub>3</sub> <sup>2-</sup>	0.0	0.0
SiO <sub>2</sub>	35.7	69.1
Salinity	37,806	36,991
Free CO <sub>2</sub>	30.30	28.4
pH	6.99	7.15
Water type	CaCl <sub>2</sub>	CaCl <sub>2</sub>

- (4) Gas sample: The CO<sub>2</sub> content of associated gas in oil reservoir A is up to 95%. After purification, the purity of CO<sub>2</sub> will be further improved to larger than 99%; hence, pure CO<sub>2</sub> (99.99%) was purchased from Yantai Deyi Gas Co., Ltd. for the experiment.

Using the above samples, two kinds of experiments were designed to investigate the CO<sub>2</sub> geochemical reaction characteristics and their effect on the rock physical properties in the target aquifers, as shown in Table 3. There are 10 sets of static CO<sub>2</sub> geochemical reaction experiments and 12 sets of thin section identification which use drill cuttings and sidewall cores, respectively. The rock samples were chosen carefully at different depths, and the reservoir samples cover good, medium, and poor physical properties, which can help us to compare the CO<sub>2</sub> geochemical reaction characteristics in the vertical direction.

**Table 3.** Experimental scheme of CO<sub>2</sub> geochemical reaction.

Aquifer	Formation	T, °C	P, MPa	Reaction Time, Day	Static Geochemical Reaction Experiment		Thin Section Identification	
					Number, Set	Rock Sample	Number, Set	Rock Sample
Aquifer Y	Caprock	52.4	8.39	7	2	Drill cuttings	3	Sidewall cores
	Reservoir	52.4	8.39	7	3	Drill cuttings	3	Sidewall cores
Aquifer H	Caprock	66.9	11.64	7	2	Drill cuttings	3	Sidewall cores
	Reservoir	66.9	11.64	7	3	Drill cuttings	3	Sidewall cores
				Total	10		12	

### 3.2. Analytical Methods

#### 3.2.1. Static CO<sub>2</sub> Geochemical Reaction Experiment

The static CO<sub>2</sub> geochemical reaction experiment aims to reveal the mineral composition change in rock induced by the CO<sub>2</sub> geochemical reaction. The main experimental equipment is shown in Figure 2. It is mainly composed of a reactor, incubator, CO<sub>2</sub> gas cylinder, and booster pump. The effective volume of the reactor is 200 mL. The maximum working pressure and working temperature are 30 MPa and 150 °C, respectively. The maximum working temperature of the thermotank is 300 °C with a control accuracy of ±0.1 °C. There are two sensors installed at the top of the reactor for P-T monitoring. The temperature sensor has a measuring range of 0–300 °C with an accuracy of ±0.1 °C, while the pressure sensor has a measuring range of 0–60 MPa with an accuracy of ±0.1 MPa. The inlet of the sampling pipeline is immersed below the gas–water interface with a filter screen to prevent cutting powder from blocking the pipeline during the sampling process.

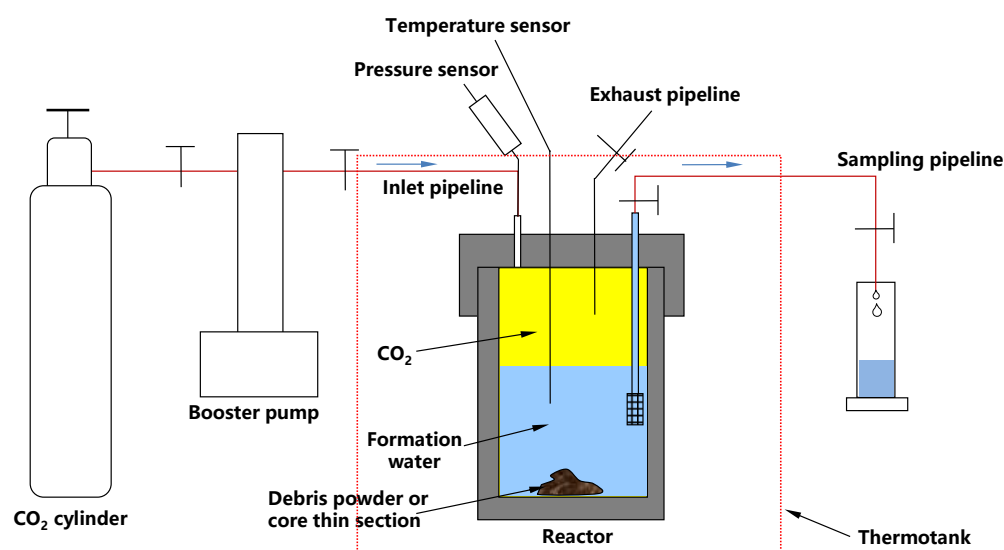


**Figure 2.** High-temperature and high-pressure CO<sub>2</sub> geochemical reaction equipment.

Limited by the contact surface area, the geochemical reaction process of CO<sub>2</sub> in the pores of rocks is usually slow. To accelerate the reaction rate and shorten the experimental time, the drill cutting samples were ground into a powder with a certain particle size before the experiment. The specific steps are as follows [38,39]:

- (1) Experimental preparation: (a) The cuttings were cleaned using deionized water to remove the residual drilling mud, dried at 90 °C, and ground into a powder with an average particle size of 200 mesh (45–125 μm) for use. (b) In total, 20 g of cutting powder was taken to analyze the mineral compositions of whole rock and clay minerals using the X-ray diffractometer (XRD) produced by PANalytical B.V. (Model X'Pert PRO MPD, Cu target, and manual mineral identification). (c) In total, 30 g of cutting powder with 150 mL of formation water was put into the reactor, the reactor was sealed with the upper air vacuumed, high-pressure CO<sub>2</sub> was injected into the reactor, and the reactor was put into the thermotank for heating; finally, the P and T of the reactor were stabilized at the design values to let the CO<sub>2</sub> react with the formation water and cutting powder.
- (2) Experimental process: (a) Each set of the CO<sub>2</sub> geochemical reaction experiments lasted for 7 days; in the meantime, the reactor was shaken several times to make sure that the bottom cutting powder was fully in contact with the formation water and CO<sub>2</sub>. (b) The formation water in the reactor was sampled on the 1st, 3rd, 5th, and 7th day, respectively, 5–10 mL at a time, and the contents of K, Na, Ca, Mg, Fe, Al, Si, and pH in the water samples were determined using the inductively coupled plasma mass

spectrometer (ICP-MS) produced by Agilent (Model 7500a, the precision is 2.7–4.6%, and the range of error is –3% to 2%).

- (3) Experimental analysis: (a) A total of 7 days later, the reactor was opened, the cutting powder after the CO<sub>2</sub> geochemical reaction was filtered, dried, and weighed, and 20 g of powder was taken for mineral composition analysis using the XRD method. (b) The CO<sub>2</sub> geochemical reaction pathway was analyzed by comparing the compositions of the cutting powder and formation water before and after the CO<sub>2</sub> geochemical reaction.

### 3.2.2. Rock Thin Section Identification before and after CO<sub>2</sub> Geochemical Reaction

Rock thin section identification can be used to observe the particle size, pore structure, and mineral composition of rocks. The original particle size and pore structure of the drill cuttings have been damaged by the drilling process, which is no longer suitable for thin section identification. Therefore, sidewall cores with similar physical properties sampled from the nearby block were used for the experiment. Because of the weak consolidation, the sidewall cores were molded into epoxy resin castings and polished into thin sections with a thickness of 0.03 mm. The German Zeiss polarized microscope (Model Axio Scope A1, ICCS optical system, 5 kinds of lens bodies with FEM design and ACR coding, maximum sample height up to 380 mm) was used to analyze the thin sections before the CO<sub>2</sub> geochemical reaction [40,41], and then the sections were placed in the reactor and immersed in the CO<sub>2</sub>-saturated formation water at the designed temperature and pressure. After 7 days of reaction, these thin sections were taken out and examined again.

### 3.2.3. Numerical Simulation of CO<sub>2</sub> Geochemical Reaction

The geochemical reaction between CO<sub>2</sub>, formation water, and rock minerals is a complex process. It is not only related to the compositions of formation water and rock minerals and the P-T conditions but also related to the contact condition and the reaction time [42]. In the CO<sub>2</sub> geochemical reaction experiment, the rock samples were ground into powder to increase the reaction surface area and accelerate the reaction rate to reach equilibrium quickly. It reflected the strong geochemical interaction between CO<sub>2</sub> and rocks, which is mainly characterized by the dissolution and formation of carbonate and clay minerals. However, each set of static CO<sub>2</sub> geochemical reaction experiments only lasted for 7 days, so it is unknown if the reaction reached the final state. Hence, referring to the experimental conditions, the GEM model of reservoir numerical simulation software CMG (v2021.10) was used to simulate the long-term CO<sub>2</sub> geochemical reaction process to verify the reasonability of the experimental results and analyze the final CO<sub>2</sub> mineral trapping potential [43]. The GEM model is multicomponent. It has a GHG function that can simulate the various CO<sub>2</sub> trapping mechanisms during its geo-storage process. For the CO<sub>2</sub> geochemical reaction simulation, the GEM model refers to the studies of Nghiem et al. who gave the main governing equations and checked the reliability [44].

According to the volume of the reactor, an equivalent geological model with a size of 7.37 cm × 7.37 cm × 7.37 cm was established. It was divided vertically into four uniform grids that can simulate the CO<sub>2</sub> dissolution and diffusion from the top to the bottom water. The porosity of the model is 50%, and the total pore volume is 200 mL. The lower 150 mL volume (three grids) is saturated with formation water, and the initial content of rock minerals for the CO<sub>2</sub> geochemical reaction is 30 g. The upper 50 mL volume (one grid) is full of CO<sub>2</sub> (Figure 3). According to the mineral composition analysis of the rock samples, three aqueous reactions and thirteen mineral reactions were mainly involved, whose commonly used reaction kinetic parameters in rock pores are shown in Tables 4 and 5, respectively [12,38,39,45]. The Henry model was used to calculate CO<sub>2</sub> solubility in formation water, and the effect of salinity was considered [46]. The CO<sub>2</sub> diffusion coefficients were set to be  $3.15 \times 10^{-9} \text{ m}^2/\text{s}$  and  $4.03 \times 10^{-9} \text{ m}^2/\text{s}$  for aquifers Y and H, respectively, estimated by the Wilke–Chang equation [47]. Based on the static contact conditions, CO<sub>2</sub> dissolution and diffusion in formation water can quickly reach stability without flow in such a small-size geological model during numerical simulation;

hence, the grid mesh will have little effect on the simulation results. Ten sets of static CO<sub>2</sub> geochemical reaction experiments were simulated, and the amount of mineralized CO<sub>2</sub> after 7 days, 10 years, 200 years, and finally 1000 years was predicted.

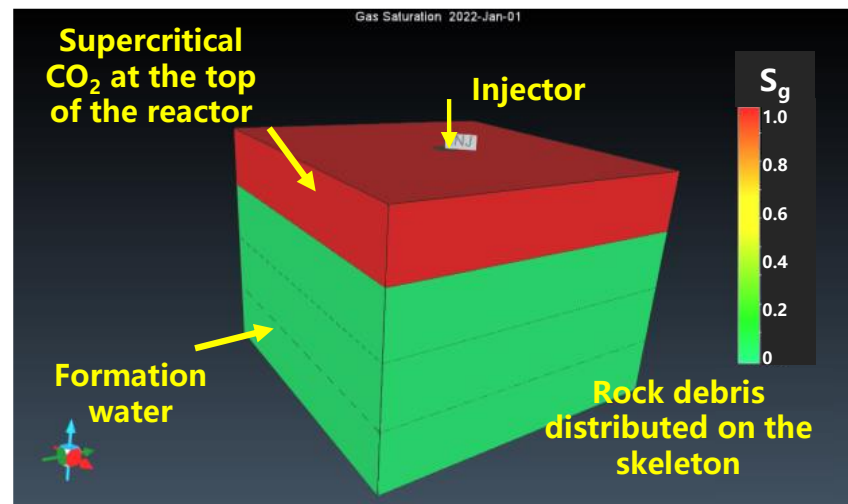


**Figure 3.** Equivalent geological model of static CO<sub>2</sub> geochemical reactor.

**Table 4.** Reaction equations and kinetic parameters of aqueous components.

No.	Reaction Equation	lgK <sub>eq</sub> <sup>a</sup> (50 °C)
1	$\text{H}_2\text{O} = \text{H}^+ + \text{OH}^-$	−13.2631
2	$\text{CO}_2(\text{aq}) + \text{H}_2\text{O} = \text{H}^+ + \text{HCO}_3^-$	−6.3221
3	$\text{CO}_2(\text{aq}) + \text{H}_2\text{O} = 2\text{H}^+ + \text{CO}_3^{2-}$	−16.5563

Table 5. Reaction equations and kinetic parameters of various minerals.

No.	Mineral	Reaction Equation	Equilibrium Constant $\lg K_{eq} = a_0 + a_1 \times t + a_2 \times t^2 + a_3 \times t^3 + a_4 \times t^4$ , Where, t Is Temperature, °C					Equilibrium Constant $\lg K_{eq}@52.4\text{ }^\circ\text{C}$	Equilibrium Constant $\lg K_{eq}@66.9\text{ }^\circ\text{C}$	Activation Energy, J/mol	Reaction Frequency Factor, $\text{mol/m}^2/\text{s}^1 @25\text{ }^\circ\text{C}$	Reaction Surface Area, $\text{m}^2/\text{m}^3$
			$a_0$	$a_1$	$a_2$	$a_3$	$a_4$					
1	Quartz SiO <sub>2</sub>	Quartz = SiO <sub>2</sub> (aq)	-4.4970	$2.1973 \times 10^{-2}$	$-1.0732 \times 10^{-4}$	$3.2461 \times 10^{-7}$	$-3.9670 \times 10^{-10}$	-3.5965	-3.4180	87,500	-13.9	7182
2	K-feldspar KAlSi <sub>3</sub> O <sub>8</sub>	K-feldspar + 4H <sup>+</sup> = 2H <sub>2</sub> O + K <sup>+</sup> + Al <sup>3+</sup> + 3SiO <sub>2</sub> (aq)	$4.6130 \times 10^{-1}$	$-1.5114 \times 10^{-2}$	$-3.8920 \times 10^{-5}$	$4.2895 \times 10^{-7}$	$-9.2187 \times 10^{-10}$	$-3.8279 \times 10^{-1}$	$-6.1408 \times 10^{-1}$	67,830	-12	176
3	Albite NaAlSi <sub>3</sub> O <sub>8</sub>	Albite + 4H <sup>+</sup> = 2H <sub>2</sub> O + Na <sup>+</sup> + Al <sup>3+</sup> + 3SiO <sub>2</sub> (aq)	3.9232	$-3.4500 \times 10^{-2}$	$2.5244 \times 10^{-5}$	$3.0994 \times 10^{-7}$	$-8.3137 \times 10^{-10}$	2.2230	1.8042	67,830	-12	250
4	Anorthite Ca [Al <sub>2</sub> Si <sub>2</sub> O <sub>8</sub> ]	Anorthite + 8H <sup>+</sup> = 4H <sub>2</sub> O + Ca <sup>2+</sup> + 2Al <sup>3+</sup> + 2SiO <sub>2</sub> (aq)	$3.1746 \times 10$	$-2.0125 \times 10^{-1}$	$5.9589 \times 10^{-4}$	$-9.0412 \times 10^{-7}$	$9.1539 \times 10^{-11}$	$2.2707 \times 10$	$2.0680 \times 10$	67,830	-12	88
5	Calcite CaCO <sub>3</sub>	Calcite + H <sup>+</sup> = Ca <sup>2+</sup> + HCO <sub>3</sub> <sup>-</sup>	2.0689	$-1.4267 \times 10^{-2}$	$-6.0610 \times 10^{-6}$	$1.4592 \times 10^{-7}$	$-4.1893 \times 10^{-10}$	1.3225	1.1226	41,870	-8.8	88
6	Dolomite CaMg(CO <sub>3</sub> ) <sub>2</sub>	Dolomite + 2H <sup>+</sup> = Ca <sup>2+</sup> + Mg <sup>2+</sup> + 2HCO <sub>3</sub> <sup>-</sup>	3.3944	$-3.5598 \times 10^{-2}$	$1.3261 \times 10^{-5}$	$2.4106 \times 10^{-7}$	$-8.1493 \times 10^{-10}$	1.5940	1.1281	41,870	-9.2218	88
7	Ankerite CaMg <sub>0.3</sub> Fe <sub>0.7</sub> (CO <sub>3</sub> ) <sub>2</sub>	Ankerite + 2H <sup>+</sup> = Ca <sup>2+</sup> + 0.3Mg <sup>2+</sup> + 2HCO <sub>3</sub> <sup>-</sup> + 0.7Fe <sup>2+</sup>	$4.4773 \times 10^{-1}$	$-2.5961 \times 10^{-2}$	$3.3916 \times 10^{-7}$	$8.9790 \times 10^{-8}$	$-3.4126 \times 10^{-10}$	$-9.0135 \times 10^{-1}$	-1.2675	46,276	-8.8	88
8	Siderite FeCO <sub>3</sub>	Siderite + H <sup>+</sup> = HCO <sub>3</sub> <sup>-</sup> + Fe <sup>2+</sup>	$2.5397 \times 10^{-1}$	$-1.9361 \times 10^{-2}$	$9.4810 \times 10^{-6}$	$1.1710 \times 10^{-7}$	$-4.1245 \times 10^{-10}$	$-7.2077 \times 10^{-1}$	$-9.7204 \times 10^{-1}$	41,870	-9.22	88
9	Pyrite FeS <sub>2</sub>	Pyrite + H <sub>2</sub> O = Fe <sup>2+</sup> + 0.25H <sup>+</sup> + 0.25SO <sub>4</sub> <sup>2-</sup> + 1.75HS <sup>-</sup>	$-2.6441 \times 10$	$7.6600 \times 10^{-2}$	$-2.8402 \times 10^{-4}$	$4.6293 \times 10^{-7}$	$-3.9254 \times 10^{-10}$	$-2.3143 \times 10$	$-2.2457 \times 10$	56.9	-4.55C	50.1
10	Illite K <sub>0.6</sub> Mg <sub>0.25</sub> Al <sub>1.8</sub> (Al <sub>0.5</sub> Si <sub>3.5</sub> O <sub>10</sub> )(OH) <sub>2</sub>	Illite + 8H <sup>+</sup> = 5H <sub>2</sub> O + 0.6K <sup>+</sup> + 0.25Mg <sup>2+</sup> + 2.3Al <sup>3+</sup> + 3.5SiO <sub>2</sub> (aq)	$1.2435 \times 10$	$-1.1227 \times 10^{-1}$	$2.7171 \times 10^{-4}$	$-8.0564 \times 10^{-8}$	$-8.3378 \times 10^{-10}$	7.2802	6.0994	58,620	-14	8573
11	Chlorite Fe <sub>2.5</sub> Mg <sub>2.5</sub> Al <sub>2</sub> Si <sub>3</sub> O <sub>10</sub> (OH) <sub>8</sub>	Chlorite + 16H <sup>+</sup> = 2.5Fe <sup>2+</sup> + 2.5Mg <sup>2+</sup> + 12H <sub>2</sub> O + 2Al <sup>3+</sup> + 3SiO <sub>2</sub> (aq)	6.6571	$-1.0170 \times 10^{-1}$	$2.0000 \times 10^{-4}$	$-2.0000 \times 10^{-7}$	$-5.0000 \times 10^{-10}$	1.8446	$6.7859 \times 10^{-1}$	62,760	-14	14,178
12	Kaolinite Al <sub>2</sub> Si <sub>2</sub> O <sub>5</sub> (OH) <sub>4</sub>	Kaolinite + 6H <sup>+</sup> = 5H <sub>2</sub> O + 2Al <sup>3+</sup> + 2SiO <sub>2</sub> (aq)	9.7295	$-9.8898 \times 10^{-2}$	$2.9156 \times 10^{-4}$	$-3.2703 \times 10^{-7}$	$-3.3110 \times 10^{-10}$	5.2983	4.3136	62,760	-13	17,600
13	Smectite Ca <sub>0.14</sub> Mg <sub>0.26</sub> Al <sub>1.77</sub> Si <sub>3.97</sub> O <sub>10</sub> (OH) <sub>2</sub>	Smectite + 6.12H <sup>+</sup> = 0.145Ca <sup>2+</sup> + 0.26Mg <sup>2+</sup> + 1.77Al <sup>3+</sup> + 3.97SiO <sub>2</sub> (aq) + 4.06H <sub>2</sub> O	$2.3304 \times 10$	$-1.2959 \times 10^{-1}$	$4.6020 \times 10^{-4}$	$-1.0434 \times 10^{-6}$	$8.4942 \times 10^{-10}$	$1.7633 \times 10$	$1.6399 \times 10$	58,620	-14	26,400

## 4. Results and Analysis

### 4.1. Mineral Composition Change Induced by CO<sub>2</sub> Geochemical Reaction

#### 4.1.1. Mineral Compositions before CO<sub>2</sub> Geochemical Reaction

The original mineral compositions of rock samples at different depths in the reservoirs and caprocks of aquifers Y and H are shown in Table 6. The whole rock mainly consists of nine kinds of minerals ranging from quartz to clay minerals, with a total composition of 100%. The clay minerals can be further divided into kaolinite, chlorite, illite, and an illite–smectite interlayer. The total content of these minerals in clay minerals is also 100%. The mineral composition of the whole rock and the composition of clay minerals are summarized in two cumulative histograms and ordered by the sample number (depth), as shown in Figure 4. The relative sizes of the different mineral contents of each rock sample at different sampling depths can be observed and compared visually.

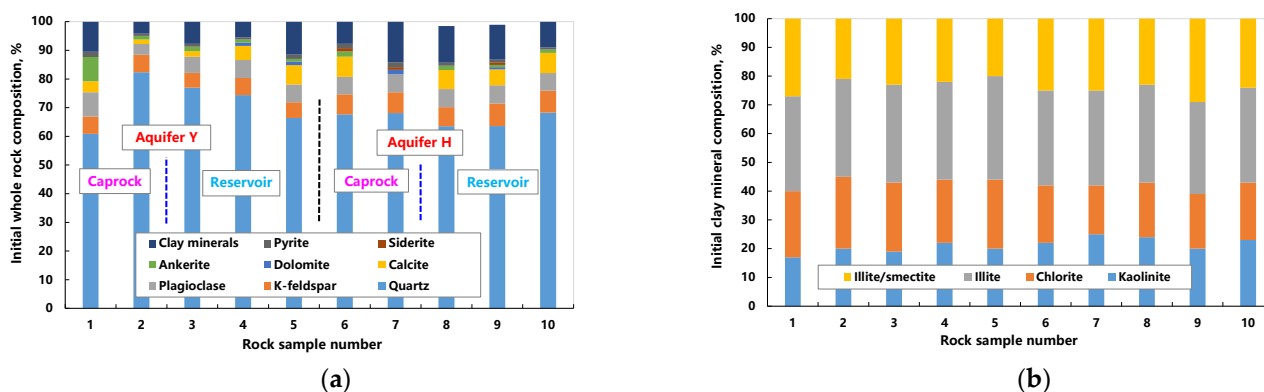


**Figure 4.** Mineral composition of each rock sample before the CO<sub>2</sub> geochemical reaction. (a) Whole rock composition. (b) Clay mineral composition.

In terms of reservoir minerals, with the increase in depth, the content of quartz, which accounts for the largest proportion in the reservoir of aquifer Y, gradually decreases from 76.97% to 66.43%, while the contents of calcite and clay minerals gradually increase, of which the content of calcite increases from 1.95% to 6.74%, and that of clay minerals from 5.46% to 11.51%. The reservoir also contains 0.9–1.52% ankerite, 1.17–1.28% dolomite, and 0.76–1.47% pyrite, while the contents of K-feldspar and plagioclase remain relatively stable, at 5.16–5.99% and 5.67–6.25%, respectively. Compared with aquifer Y, the clay mineral content in the reservoir of aquifer H is larger, which decreases from 12.78% to 9% with the increase in depth, while the calcite content remains relatively stable at 5.55–6.63%, the ankerite content is 0.79–1.55%, the pyrite content is 0.72–1.06%, and some of its rock samples also contain 0.9% siderite. In addition, the contents of the four minerals in clay minerals are stable. In the reservoir of aquifer Y, the contents of kaolinite, chlorite, illite, and the illite–smectite interlayer are 19–22%, 22–24%, 34–36%, and 20–23%, respectively. The corresponding clay mineral contents in the reservoir of aquifer H are 20–24%, 19–20%, 32–34%, and 23–29%, respectively, which are similar to those in aquifer Y.

In terms of caprock minerals, as the depth increases, the quartz content in the caprock of aquifer Y increases from 60.86% to 82.37%, the clay mineral content decreases from 10.52% to 4.2%, and the calcite and ankerite contents decrease from 3.84% and 8.42% to 1.58% and 1.26%, respectively. In the caprock of aquifer H, the quartz content is relatively stable, at 67.7–68.14%, and the content of clay minerals increases from 7.75% to 14.14%. The upper caprock contains 7% calcite and 1.84% ankerite, while the lower caprock only contains 1.47% calcite. The compositions of the clay minerals in the caprocks of aquifers Y and H are also relatively stable.

In general, the main mineral of the reservoirs and caprocks of aquifers Y and H is quartz. The contents of plagioclase and K-feldspar are relatively stable, while those of easily reactive minerals such as carbonate and clay are relatively high. The mineral compo-

sitions in the reservoirs have an obvious relationship with depth and the heterogeneity is small, while the mineral contents in the caprocks vary significantly with depth, and the heterogeneity is strong. In addition, it should be noted that the rock samples evaluated are generally high in clay minerals and that there was no significant difference in the clay contents of the reservoir and caprock, which may be related to the fact that the drilling debris is a mixture collected along a well section and might have been contaminated with drilling mud.

#### 4.1.2. Mineral Compositions after CO<sub>2</sub> Geochemical Reaction

Following the experimental scheme, ten rock samples reacted with formation water and CO<sub>2</sub> for 7 days under the target aquifer conditions. The mineral compositions after the CO<sub>2</sub> geochemical reaction were measured, as shown in Table 7. In order to compare the content change in each mineral of each rock sample induced by the geochemical reaction conveniently, the mineral content after the geochemical reaction was subtracted from the mineral content before, and the minerals that increased and decreased in content were added up separately, and finally, two cumulative histograms of the mineral composition change in each rock sample at different depths were plotted in Figure 5. In addition, due to the great difference in the concentration between different ions in formation water, which vary from tens of thousands mg/L to several mg/L, it is hard to show the details of ions with a low concentration when all the ions are drawn in one figure. Therefore, the ratio of the measured value to the initial value was used to present the concentration change in each ion over time during the CO<sub>2</sub> geochemical reaction, as shown in Figure 6.

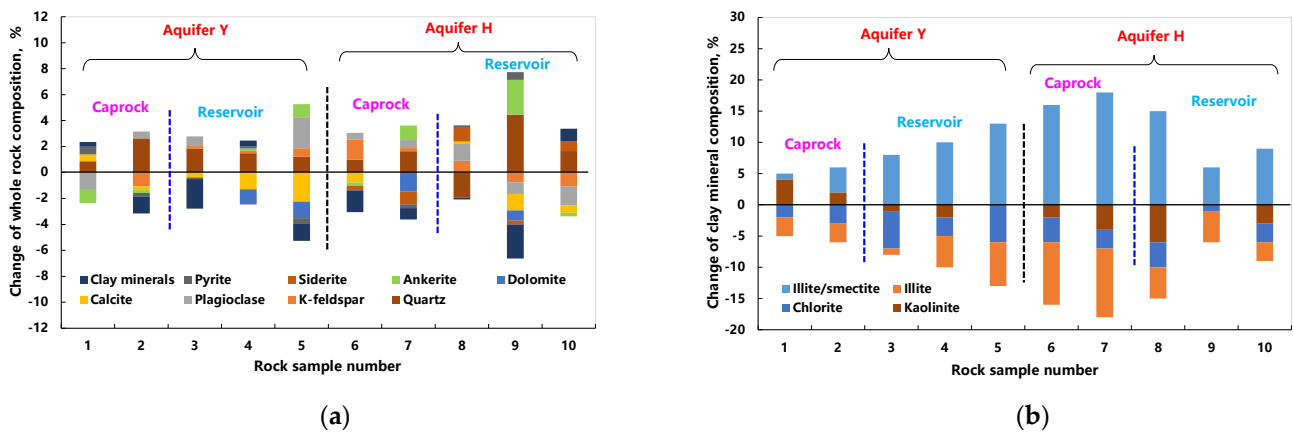


Figure 5. Mineral composition changes in each rock sample after the CO<sub>2</sub> geochemical reaction. (a) Change in whole rock composition. (b) Change in clay mineral composition.

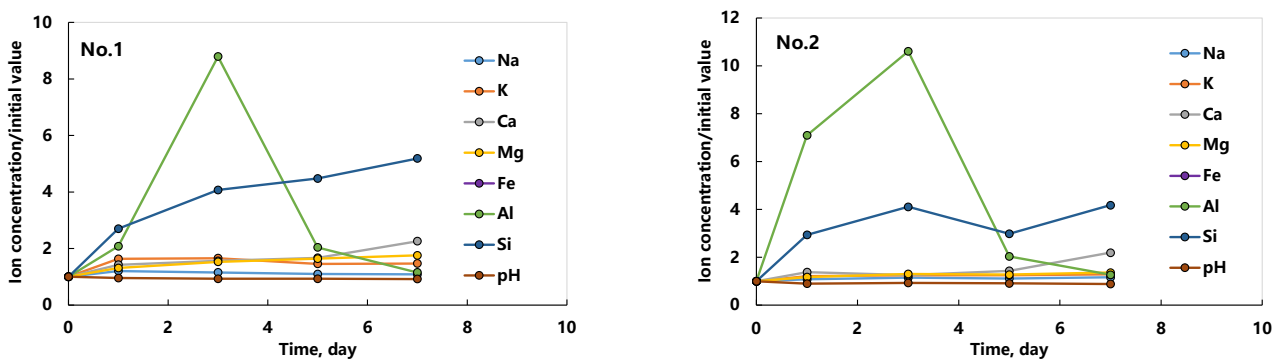


Figure 6. Cont.

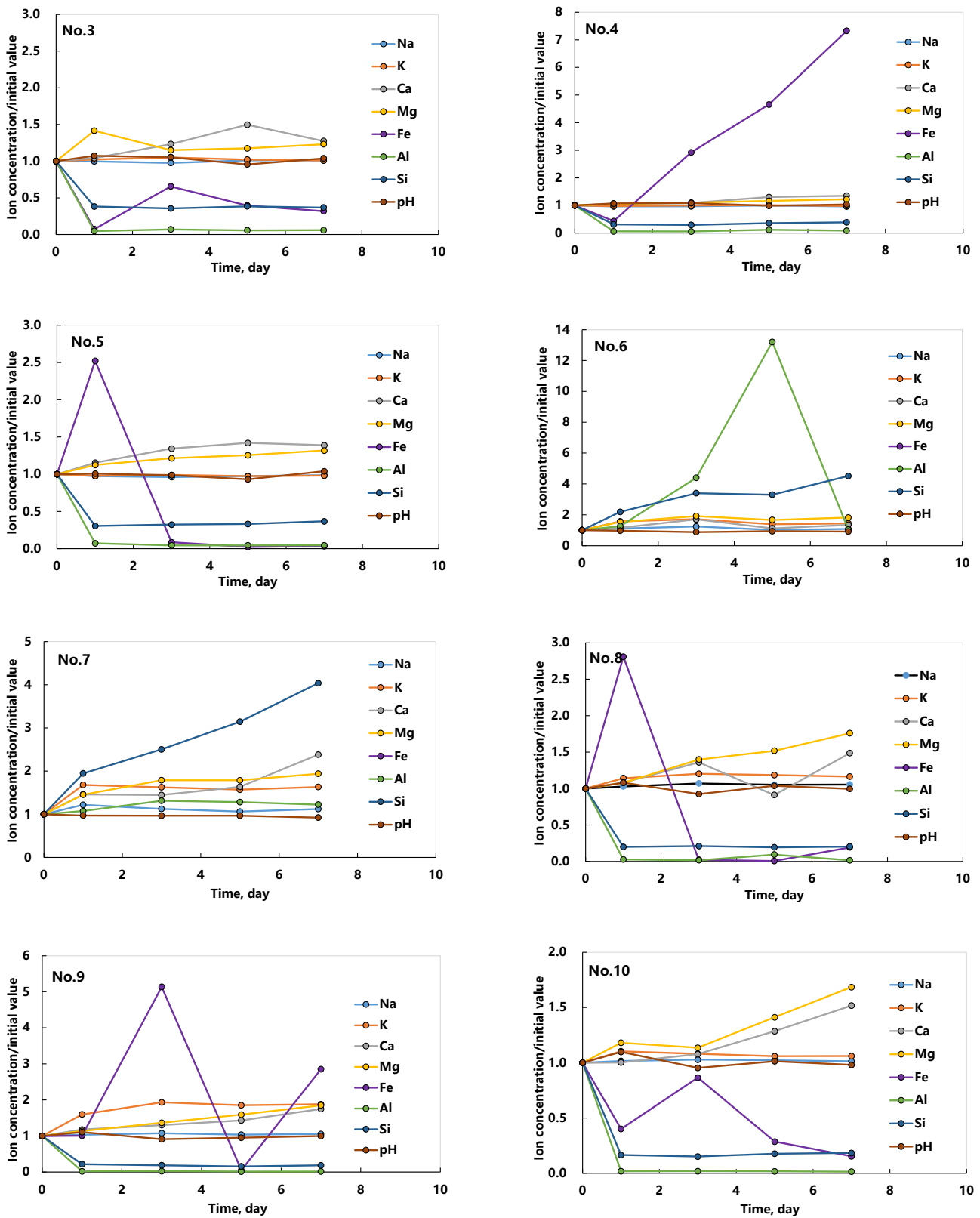


Figure 6. Concentration changes in ions in formation water with the CO<sub>2</sub> geochemical reaction time.

**Table 6.** Mineral compositions of rock samples before the CO<sub>2</sub> geochemical reaction.

Sample #	Mineral Composition of Whole Rock, %								Composition of Clay Minerals, %				
	Quartz	K-FELDSPAR	Plagioclase	Calcite	Dolomite	Ankerite	Siderite	Pyrite	Clay Minerals	Kaolinite	Chlorite	Illite	Illite/Smectite
1	60.86	6.03	8.5	3.84	-	8.42	-	1.83	10.52	17	23	33	27
2	82.37	6.06	3.76	1.58	-	1.26	-	0.77	4.2	20	25	34	21
3	76.97	5.16	5.67	1.95	-	1.52	-	1.03	7.7	19	24	34	23
4	74.39	5.99	6.25	4.93	1.17	1.05	-	0.76	5.46	22	22	34	22
5	66.43	5.46	6.21	6.74	1.28	0.9	-	1.47	11.51	20	24	36	20
6	67.7	6.98	6.08	7	-	1.84	1.2	1.45	7.75	22	20	33	25
7	68.14	7.24	6.32	-	1.47	-	0.98	1.71	14.14	25	17	33	25
8	63.54	6.63	6.31	6.63	-	1.5	-	1.06	12.78	24	19	34	23
9	63.59	7.85	6.36	5.55	0.79	0.79	0.9	0.91	12.16	20	19	32	29
10	68.28	7.67	6.12	7.06	-	1.15	-	0.72	9	23	20	33	24

Note: 1–2 are caprock samples of aquifer Y, 3–5 are reservoir samples from aquifer Y, 6–7 are caprock samples from aquifer H, and 8–10 are reservoir samples from aquifer H.

**Table 7.** Mineral compositions of rock samples after the CO<sub>2</sub> geochemical reaction.

Sample #	Mineral Composition of Whole Rock, %								Composition of Clay Minerals, %			
	Quartz	K-Feldspar	Plagioclase	Calcite	Ankerite	Siderite	Pyrite	Clay Minerals	Kaolinite	Chlorite	Illite	Illite/Smectite
1	61.73	6.01	7.18	4.37	7.41	-	2.42	10.88	21	21	30	28
2	85	5	4.29	1.28	1.04	-	0.5	2.89	22	22	31	25
3	78.79	5.38	6.41	1.57	1.52	-	0.9	5.43	18	18	33	31
4	75.87	6.18	6.16	3.73	1.24	-	0.9	5.92	20	19	29	32
5	67.64	6.12	8.55	4.5	1.95	-	1.08	10.16	20	18	29	33
6	68.7	8.52	6.59	6.23	1.57	0.9	1.41	6.08	20	16	23	41
7	69.78	7.48	6.94	-	1.12	-	1.42	13.26	21	14	22	43
8	61.6	7.54	7.65	6.75	1.52	1.11	1.19	12.64	18	15	29	38
9	68.04	7.1	5.46	4.28	3.48	0.6	1.5	9.54	20	18	27	35
10	69.93	6.59	4.69	6.46	0.88	0.71	0.78	9.96	20	17	30	33

For the rock samples in the reservoir of aquifer Y, after 7 days of the CO<sub>2</sub> geochemical reaction, most of the carbonate minerals such as calcite and dolomite, and some of the clay minerals, were dissolved. Accordingly, the contents of quartz, K-feldspar, and plagioclase increased. Some of the rock samples also generated a small amount of ankerite and clay minerals. The contents of kaolinite, chlorite, and illite in the clay minerals decreased, while the content of the illite-smectite interlayer increased. In addition, the concentrations of Na<sup>+</sup> and K<sup>+</sup> in formation water were stable during the CO<sub>2</sub> geochemical reaction, but those of ions with a small content changed greatly, which are sensitive to the geochemical reaction. The dissolution of carbonate minerals can make the Ca<sup>2+</sup> and Mg<sup>2+</sup> concentrations gradually increase and tend to be stable. The formation of feldspar and quartz can cause the decrease in the Al<sup>3+</sup> and Si concentrations, and the Fe (Fe<sup>2+</sup> + Fe<sup>3+</sup>) concentration varied significantly. Among them, the Fe in the water of No. 4 and No. 5 rock samples increased, corresponding to the formation of a small amount of ankerite.

For the rock samples in the reservoir of aquifer H, after 7 days of the CO<sub>2</sub> geochemical reaction, most of the carbonate minerals, K-feldspar, and plagioclase in the rock samples were dissolved, and additional quartz, siderite, and ankerite were generated accordingly. Among them, the clay content of rock sample No. 9 (mudstone interlayer) decreased significantly, while the quartz content increased markedly. The changes in the clay mineral composition are similar to those of the aquifer Y. Due to the dissolution of feldspar and clay minerals, the concentrations of Na<sup>+</sup> and K<sup>+</sup> in formation water increased slowly and reached stability, especially the K<sup>+</sup> concentration, which in the case of the mudstone interlayer increased significantly. The dissolution of carbonate minerals caused a gradual increase in the Ca<sup>2+</sup> and Mg<sup>2+</sup> concentrations in water, while the formation of siderite and dolomite led to the overall decrease in the Fe concentration, and the formation of quartz and clay minerals led to decline in the Al<sup>3+</sup> and Si concentrations in water.

For the rock samples in the caprock of aquifer Y, after 7 days of the CO<sub>2</sub> geochemical reaction, the ankerite and plagioclase in the upper caprock were dissolved, forming quartz, calcite, and clay minerals, while the dissolution of clay minerals, calcite, ankerite, and K-feldspar dominated in the lower caprock, forming more quartz and plagioclase. For the clay mineral composition in the upper and lower caprocks, the contents of illite and chlorite decreased, while those of kaolinite and the illite-smectite interlayer increased. Accordingly, with the geochemical reaction, the concentrations of Na<sup>+</sup> and K<sup>+</sup> in formation water increased first and then quickly stabilized, while the concentrations of Ca<sup>2+</sup> and Mg<sup>2+</sup> gradually increased, and there was still an upward trend after 7 days. In addition, the concentration of Al<sup>3+</sup> increased first and then decreased rapidly, while the concentration of Si gradually increased.

For the rock samples in the caprock of aquifer H, after 7 days of the CO<sub>2</sub> geochemical reaction, the dissolution of clay minerals, siderite, ankerite, and calcite in the upper caprock mainly occurred to form quartz, K-feldspar, and plagioclase, while in the lower caprock, the clay minerals, dolomite, and siderite were dissolved, and the quartz, ankerite, and a small amount of feldspar formed. The content of the illite-smectite interlayer in the clay minerals both in the upper and lower caprocks increased significantly. In formation water, except for the small change in the Al<sup>3+</sup> concentration in the lower caprock, the changes in each ion in the water of upper and lower caprocks are similar to those of the caprocks of aquifer Y.

To sum up, it can be seen that with the CO<sub>2</sub> geochemical reaction, the contents of quartz and feldspar in aquifers Y and H will increase, while those of calcite, dolomite, and clay minerals will decrease. The contents of carbonate and clay minerals in the reservoir of aquifers are relatively high, which are prone to causing dissolution reactions. The contents of typical ions, including Ca<sup>2+</sup> and Mg<sup>2+</sup> in formation water, can increase obviously, and the change in the mineral composition after the geochemical reaction will also be great. Comparatively, the original mineral compositions of aquifer caprocks are quite different. They will change slightly after the geochemical reaction, but the geochemical reaction process is more complicated. The specific process of the geochemical reaction should be

determined by the compositions of minerals and formation water, as well as the kinetic parameters of the reaction [48].

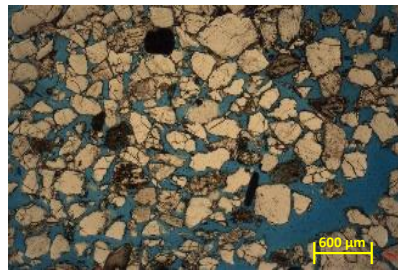
#### 4.2. Rock Micromorphology Change Induced by CO<sub>2</sub> Geochemical Reaction

##### 4.2.1. Thin Section Analysis before CO<sub>2</sub> Geochemical Reaction

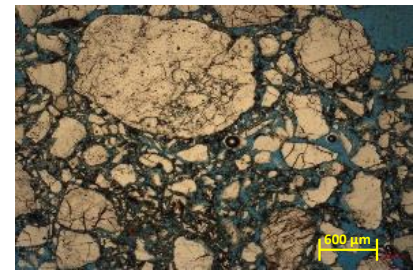
In order to obtain the original rock micromorphology, a thin section identification of sidewall cores sampled at different depths in aquifers Y and H was conducted before the CO<sub>2</sub> geochemical reaction. The micrographs of the thin sections are shown in Figures 7 and 8.



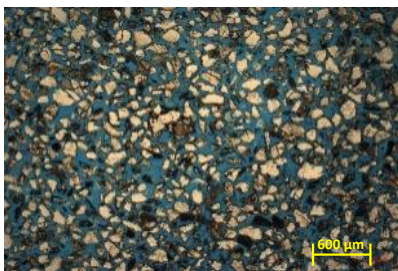
No. 4: Upper reservoir, poor physical properties, aquifer Y.



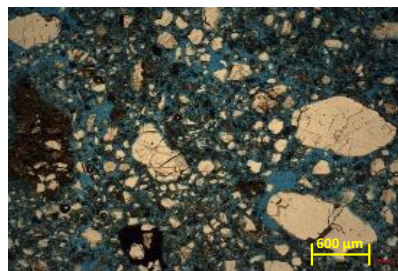
No. 5: Middle reservoir, good physical properties, aquifer Y.



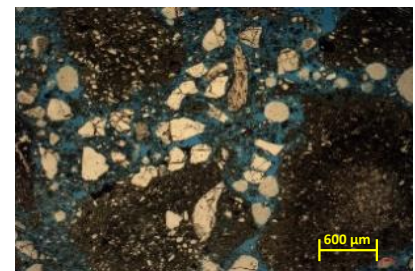
No. 6: Lower reservoir, medium physical properties, aquifer Y.



No. 10: Upper reservoir, good physical properties, aquifer H.

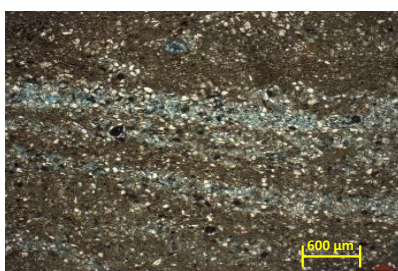


No. 11: Middle reservoir, poor physical properties, aquifer H.



No. 12: Lower reservoir, medium physical properties, aquifer H.

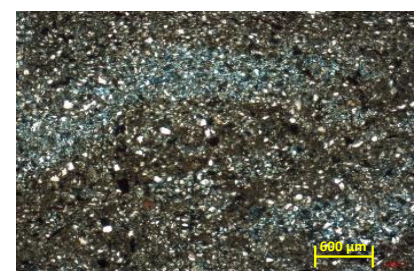
**Figure 7.** Microphotographs of reservoir cores before the CO<sub>2</sub> geochemical reaction.



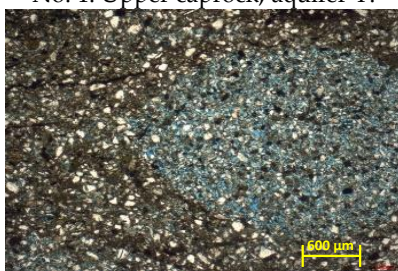
No. 1: Upper caprock, aquifer Y.



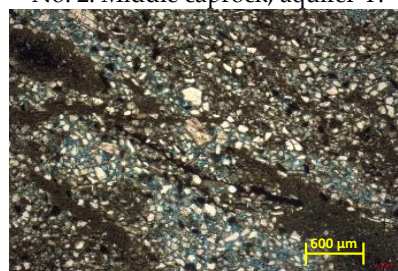
No. 2: Middle caprock, aquifer Y.



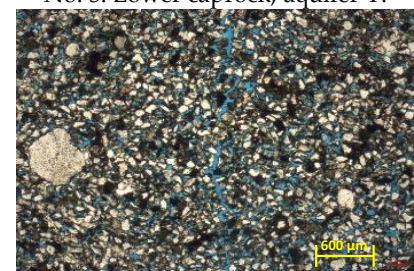
No. 3: Lower caprock, aquifer Y.



No. 7: Upper caprock, aquifer H.



No. 8: Middle caprock, aquifer H.



No. 9: Lower caprock, aquifer H.

**Figure 8.** Microphotographs of caprock cores before the CO<sub>2</sub> geochemical reaction.

The thin section identification of reservoir cores shows that the reservoirs of aquifers Y and H are mainly made up of medium-to-fine-grained sandstones with feldspathic quartz, and a small number of rock samples are pebbly siltstone with lithic quartz. The reservoir rocks have a detrital structure. The content of detrital grains is up to 66–88%, which are mainly quartz and feldspar, associated with a small amount of biological debris in some rock samples. The intergranular fillings are mainly clay, dolomite, and calcite with a total content of only 3–10%, but in some rock samples, the content of dolomite in the fillings is up to 25%. Comparatively, the reservoir of aquifer H contains more clay matrix than that of aquifer Y. The rocks are mostly porous and poorly sorted. The intergranular pores are mainly original pores with a small number of dissolved pores. The pore size is 50–200  $\mu\text{m}$ , and the total porosity is usually 9–29%, while in some cases it is 0.5–3.5%.

The thin section identification of caprock cores shows that the caprocks of aquifers Y and H mainly consist of fine-grained felsic sedimentary rocks. The felsic detrital grains and argillaceous, siliceous, and ferruginous fillings are deposited together with the felsic detrital grains locally enriched in pellets. The rock samples have a fine-grained detrital structure. The main minerals of the detrital grains are quartz, feldspar, and biotite (a few samples contain biological debris), accounting for about 55–80%. The intergranular pores are filled with argillaceous, siliceous, calcareous, and dolomite minerals, with a total content of 14–40%. They are of basal cementation with good grain sorting. The intergranular pores are mainly original pores, the pore size is 50–100  $\mu\text{m}$ , and the total porosity is 1–6%.

Based on the above analysis, it can be seen that the physical properties of the reservoirs and caprocks of aquifers Y and H are very different. The reservoirs have detrital grains with a large size, distinct outline, poor sorting, low filling content, and large intergranular pores, which can provide favorable space for  $\text{CO}_2$  storage. Comparatively, the caprocks contain a low content of detrital grains with a small size and a high content of argillaceous, siliceous, and ferruginous fillings with basal cementation and good sorting, which can have a good sealing effect on  $\text{CO}_2$  storage.

#### 4.2.2. Thin Section Analysis after $\text{CO}_2$ Geochemical Reaction

After 7 days of the  $\text{CO}_2$  geochemical reaction under formation conditions, the 12 thin sections were investigated once again, and the micrographs of these core thin sections are shown in Figures 9 and 10. The thin section identification of reservoir cores shows that after the  $\text{CO}_2$  geochemical reaction, the carbonate minerals such as calcite and dolomite in the reservoir rocks were dissolved. The number of intergranular pores was increased, and the siliceous content was enhanced by 2–4%. In addition, in the rock samples of No. 4 and No. 6, the content of clay minerals was increased, and the thin section color became deeper. The porosity of the No. 5 rock sample was increased from 13% to 15%, while that of the No. 11 and No. 12 rock samples was decreased from 10% and 15% to 5% and 10%, respectively.

The thin section identification of caprock cores show that after the  $\text{CO}_2$  geochemical reaction, the calcite and dolomite in the caprocks of aquifer Y were also dissolved and both the content of clay minerals and the porosity were increased slightly. In the caprocks of aquifer H, the dolomite was dissolved, and the siliceous content of some rock samples was also decreased. Accordingly, the porosity was increased, which may decrease the breakthrough pressure of caprock and increase the risk of  $\text{CO}_2$  leakage.

#### 4.3. $\text{CO}_2$ Mineral Trapping Capacity by Geochemical Reaction

The  $\text{CO}_2$  mineral trapping mechanism refers to the process where the divalent cations such as Ca, Mg, and Fe are released from non-carbonate minerals and react with  $\text{CO}_2$  to generate carbonate minerals for storage. Hence, from this point of view, the theoretical maximum  $\text{CO}_2$  mineral trapping capacity is the amount of  $\text{CO}_2$  required to convert all Ca, Mg, and Fe in the non-carbonate minerals into carbonate minerals. This parameter is often used for the preliminary assessment of  $\text{CO}_2$  mineral trapping potential [12]. In aquifers Y and H, the main non-carbonate minerals containing Ca, Mg, and Fe are anorthite, pyrite,

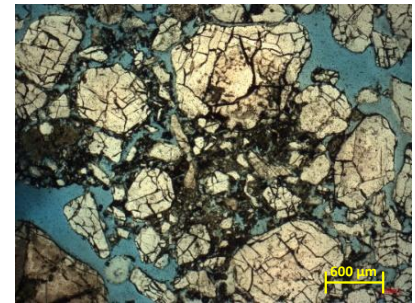
illite, chlorite, and smectite. The theoretical maximum CO<sub>2</sub> mineral trapping capacities of the rock samples were calculated to be 0.023–0.0538 mol/100 g rock. There is no significant difference in the calculated results of the caprocks and reservoirs of the two aquifers.



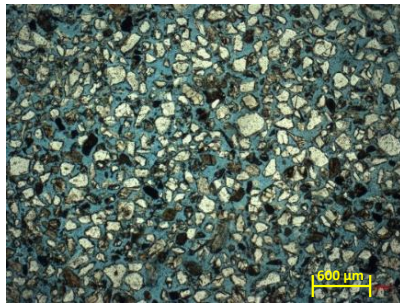
No. 4: Upper reservoir, poor physical properties, aquifer Y.



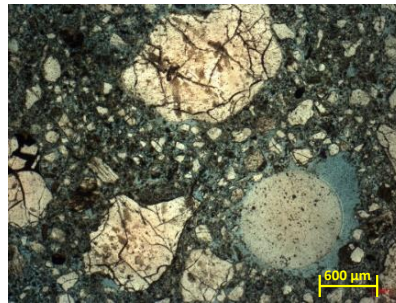
No. 5: Middle reservoir, good physical properties, aquifer Y.



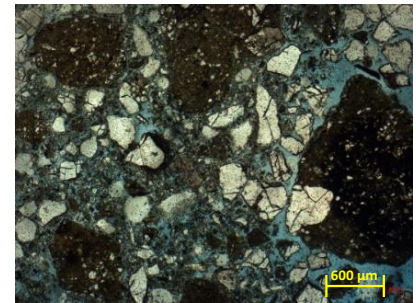
No. 6: Lower reservoir, medium physical properties, aquifer Y.



No. 10: Upper reservoir, good physical properties, aquifer H.



No. 11: Middle reservoir, poor physical properties, aquifer H.

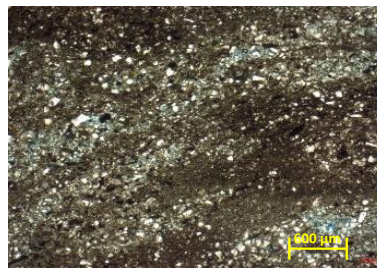


No. 12: Lower reservoir, medium physical properties, aquifer H.

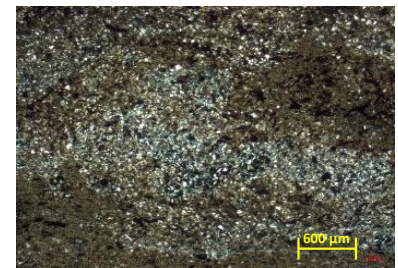
**Figure 9.** Microphotographs of reservoir cores after the CO<sub>2</sub> geochemical reaction.



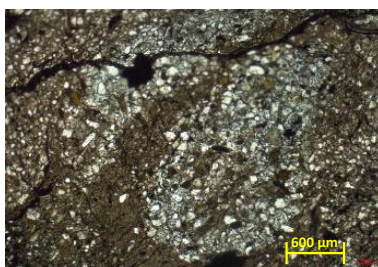
No. 1: Upper caprock, aquifer Y.



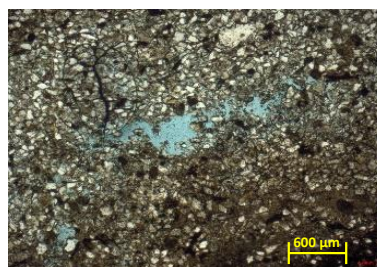
No. 2: Middle caprock, aquifer Y.



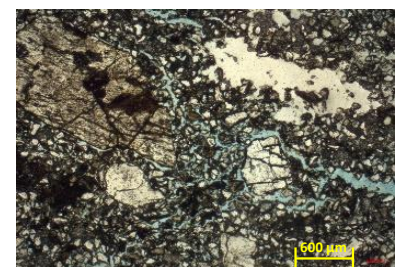
No. 3: Lower caprock, aquifer Y.



No. 7: Upper caprock, aquifer H.



No. 8: Middle caprock, aquifer H.



No. 9: Lower caprock, aquifer H.

**Figure 10.** Microphotographs of caprock cores after the CO<sub>2</sub> geochemical reaction.

However, under the actual formation conditions, because of the dynamic equilibrium process of the geochemical reaction, only part of Ca, Mg, and Fe in the non-carbonate minerals can be released, and only part of them can convert into carbonate minerals.

Meanwhile, part of the original carbonate minerals may be dissolved and release CO<sub>2</sub>. As a result, the real utilization factor of the theoretical maximum CO<sub>2</sub> mineral trapping capacity is not high. This factor can be determined by experimental or numerical methods. Hence, the amount of mineralized CO<sub>2</sub> in the static geochemical reaction experiment was calculated based on the composition change in the carbonate minerals before and after the geochemical reaction (including calcite, dolomite, ankerite, and siderite). The amount of mineralized CO<sub>2</sub> after different reaction times was predicted using the GEM model. All these results are shown in Table 8 and Figure 11. Since the geochemical reaction of CO<sub>2</sub> was simulated under the porous condition, the reaction surface area of each mineral is relatively small, and the reaction rate is also slow. Therefore, after 7 days of reaction, the change in the mineral composition and the CO<sub>2</sub> mineralized amount is small. But with the reaction time extension, the geochemical reaction can reach stability after 200 years. Most of the rock samples own the dissolution feature of carbonate minerals, and the amount of mineralized CO<sub>2</sub> is usually negative. By comparison, the experimental results (reaction for 7 days) are close to the predicted values after 10 years, which cannot represent the final state. In the final state (1000 years later), only three rock samples can realize the effective utilization of the theoretical maximum CO<sub>2</sub> mineral trapping capacity, and the largest utilization factor is 75% (utilization factor = predicted final value/theoretical max. value), while the other rock samples all provide negative values. The average utilization factor is only −55.43%. Overall, under the reactor conditions, the mineralized CO<sub>2</sub> amount only accounts for −0.32%, which can be ignored, while the dissolved CO<sub>2</sub> and supercritical CO<sub>2</sub> account for 33.46% and 66.85%, respectively.

Table 8. Amounts of mineralized CO<sub>2</sub> and the utilization factors of rock samples.

No.	Theoretical Max. Value	Experimental Value (after 7 Days)	Predicted Value				Final Utilization Factor, %
			7 Days	10 Years	200 Years	Finally	
1	0.0538	−0.0042	−0.0010	0.0063	0.0264	0.0264	49.15
2	0.0230	−0.0049	−0.0008	−0.0066	0.0007	0.0055	23.78
3	0.0365	−0.0034	−0.0011	0.0047	−0.0329	−0.0329	−90.19
4	0.0292	−0.0221	−0.0011	−0.0638	−0.0625	−0.0625	−213.79
5	0.0498	−0.0239	−0.0012	−0.0106	−0.0355	−0.0355	−71.22
6	0.0385	−0.0132	−0.0015	−0.0047	−0.0436	−0.0491	−127.39
7	0.0500	−0.0136	−0.0006	0.0008	0.0217	0.0368	73.55
8	0.0446	0.0122	−0.0006	−0.0110	−0.0433	−0.0433	−97.04
9	0.0421	−0.0276	−0.0015	−0.0091	−0.0412	−0.0412	−97.86
10	0.0349	−0.0015	−0.0013	−0.0034	−0.0011	−0.0011	−3.28

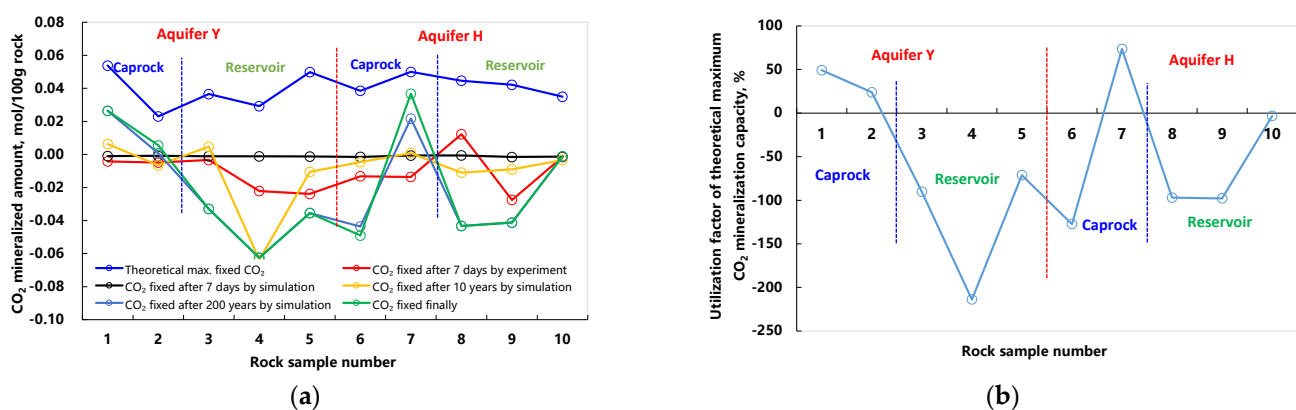


Figure 11. Amounts of mineralized CO<sub>2</sub> and the utilization factors of rock samples. (a) Amount of mineralized CO<sub>2</sub>. (b) Utilization factor of theoretical maximum CO<sub>2</sub> mineral trapping capacity.

## 5. Discussion

In this study, laboratory experiments and numerical simulations were carried out to study the characteristics of CO<sub>2</sub> geochemical reactions in the target saline aquifers. Some research experiences have been obtained. First, 200 mesh rock powder was used in the static CO<sub>2</sub> geochemical reaction experiment, aiming to quickly obtain the final equilibrium state of the CO<sub>2</sub> geochemical reaction. However, the experimental results obtained after 7 days of the reaction are equivalent to the results after 10 years of numerical simulation, which is not the final state. This indicates that a longer reaction time or finer ground rock powder may be required in future experiments to reach reaction equilibrium. Because the experimental conditions of the static CO<sub>2</sub> geochemical reaction are different from the real formation, the numerical simulation was mainly conducted to observe the performance of the geochemical reaction at different equilibrium degrees. The effects of mineral composition, reaction time, and P-T conditions were all involved in the experiment. This is similar to the sensitivity analysis of the influencing factors. However, due to the complexity of the geochemical reaction, the law of the geochemical reaction obtained was not obvious, but rather it indicates that the reaction was dominated by mineral dissolution. Comparatively, it is more meaningful to conduct and fit the dynamic geochemical reaction experiment which uses intact cores for flooding.

The CO<sub>2</sub> geochemical reaction can not only provide the CO<sub>2</sub> mineral trapping potential but also change the aquifer's physical properties, affecting the law of CO<sub>2</sub> seepage and the safety of structural trapping. In this study, the aquifers Y and H are located offshore with a shallow buried depth, and the content of carbonate and clay minerals is relatively high. This study has shown that the dissolution of carbonate minerals will dominate in the aquifers when CO<sub>2</sub> is injected. Calcite, dolomite, and clay minerals mainly dissolve, while quartz and feldspar are mainly produced, and the corroded pore number and porosity will increase. The contribution of mineral trapping to the CO<sub>2</sub> storage potential is negative, which can be ignored, but the impact of the geochemical reaction on the physical properties of the reservoir and caprock needs to attract more attention. The results obtained in this study are in good agreement with the published literature. A large number of studies have been conducted on caprock sealing performance under the effect of a CO<sub>2</sub> geochemical reaction. Alemu et al. [49] used a high-temperature and high-pressure reactor to carry out an experiment of CO<sub>2</sub> breakthrough in caprock under static conditions and obtained a change in the rule of the micro-structure properties and mineral dissolution of the caprock before and after the reaction. Wollenweber et al. [50] conducted experimental studies on the seepage, diffusion, and water-rock reaction of CO<sub>2</sub> in caprocks and found that the effective diffusion coefficient of CO<sub>2</sub> increased due to the change in the caprock's minerals and pore structure. Through experiment and numerical simulation, Gherardi et al. [51] studied the changes in the physical properties of the caprocks after CO<sub>2</sub> injection and concluded that CO<sub>2</sub> would produce chemical dissolution on the caprocks, thus reducing the sealing effect of the caprocks and increasing the CO<sub>2</sub> leakage risk. Luquot and Gouze [52] observed the phenomenon of increased permeability caused by mineral dissolution in the experiment of a CO<sub>2</sub> geochemical reaction. In the studies of Kim et al. and Yang et al. [53,54], it was also observed that a CO<sub>2</sub> geochemical reaction can lead to different changes in porosity and permeability at different locations; in their studies, the mineral dissolution of calcite and dolomite mainly occurred upstream, while carbonate mineral precipitation mainly occurred downstream, showing different geochemical reaction characteristics in the lower and upper caprock. In general, CO<sub>2</sub> geochemical reactions can dissolve caprocks, the size of the pore throat may increase, the existing cracks may further develop, and the fault may be activated; all of these can reduce the caprock sealing performance and cause CO<sub>2</sub> leakage.

It should be noted that the physical properties of weakly consolidated saline aquifers are more easily affected by CO<sub>2</sub> geochemical reactions, which can further damage CO<sub>2</sub> storage safety significantly. According to the investigation, the geological sedimentary age of offshore saline aquifers buried at a depth of 1000–3000 m in China is generally young [55]. The compaction of the formation rock is weak. Most of them are medium-to-

high permeability reservoirs with typical mud-sand interlayers and strong heterogeneity, but the rocks are often weak and easily broken. These geological characteristics will significantly affect the migration and trapping process of CO<sub>2</sub> in saline aquifers, and the CO<sub>2</sub> geochemical reaction may also cause formation deformation and caprock failure. Therefore, it is very necessary to carry out detailed studies on saline aquifers with such geological conditions to reveal the effect of CO<sub>2</sub> geochemical reactions on storage safety.

## 6. Conclusions

- (1) Saline aquifers Y and H are marine weakly consolidated sandstone formations. The reservoirs are mostly made up of fine-to-medium-grained sandstones as quartz arenite with a considerable amount of feldspar. The detrital grains have a large size, distinct outline, poor sorting, low content of fillings, and large intergranular pores, which can provide favorable pore space for CO<sub>2</sub> storage. Comparatively, the caprocks contain a low content of detrital grains with a small size and a high content of argillaceous, siliceous, and ferruginous fillings with a basal cementation and good sorting, which can has a good sealing effect on CO<sub>2</sub> storage.
- (2) Both the reservoirs and caprocks of aquifers Y and H contain a certain amount of carbonate and clay minerals. When CO<sub>2</sub> is injected into aquifers, mineral dissolution will dominate. The contents of quartz and feldspar will increase, while the contents of calcite, dolomite, and clay minerals will decrease. At the same time, more Ca<sup>2+</sup> and Mg<sup>2+</sup> will be released into the formation water. Due to the different original mineral compositions, the CO<sub>2</sub> geochemical reaction is more complicated in caprocks. The specific CO<sub>2</sub> geochemical reaction process is determined jointly by the mineral composition, the ion concentrations, the contact surface, the P-T conditions, and the reaction time.
- (3) Aquifers Y and H have a theoretical maximum CO<sub>2</sub> mineral trapping capacity of 0.023–0.0538 mol/100 g rock, but due to the dynamic equilibrium of the geochemical reaction, only a small number of rock samples can realize the effective utilization of this theoretical capacity, and the largest utilization factor is 75%, while the average utilization factor is only –55.43%. Overall, the amount of mineralized CO<sub>2</sub> is negative, and the contribution of mineral trapping to CO<sub>2</sub> storage capacity takes –0.32%, which can be ignored.
- (4) CO<sub>2</sub> geochemical reaction can not only provide the CO<sub>2</sub> mineral trapping potential but also change the aquifer's physical properties and affect the law of CO<sub>2</sub> seepage and the safety of CO<sub>2</sub> storage. It is very necessary to conduct systematic and detailed research in the future to reveal the effect of geochemical reactions on CO<sub>2</sub> storage safety, especially in offshore weakly consolidated sandstone saline aquifers which could be important potential sites for large-scale CO<sub>2</sub> storage in China.

**Author Contributions:** Conceptualization, M.X.; methodology, Z.T.; validation, X.S.; investigation, Z.Y.; resources, S.F.; data curation, X.S.; writing—review and editing, F.L. and L.Z.; visualization, D.Z.; supervision, L.Z. All authors have read and agreed to the published version of the manuscript.

**Funding:** This research is supported by the Research Project of CNOOC China Limited (YXKY-SXSH-2021-SZ-01).

**Data Availability Statement:** We state that the data are unavailable due to the privacy or ethical restrictions of the company and university.

**Acknowledgments:** We appreciate the reviewers and editors for their constructive comments contributing to this paper's high quality.

**Conflicts of Interest:** Authors Mingying Xie, Zhiyong Tu, Xiaona Sun, Zhenghe Yan, and Shasha Feng are employees of the company Shenzhen Branch of CNOOC China Limited. The remaining authors declare that the research was conducted in the absence of any commercial or financial relationships that could be construed as potential conflicts of interest.

## References

1. Zhu, W.Q.; Wang, Q. Key Technologies and prospects for the construction of global energy Internet under the background of carbon neutral. *Power Gen. Technol.* **2021**, *42*, 3–7. (In Chinese with English Abstract)
2. Liu, P.; Yang, W.H.; Zhang, J.; Sun, H.R.; Cui, Z.X. Prospects for emission reduction technologies under carbon neutral targets. *Mod. Chem. Ind.* **2021**, *41*, 6–10. (In Chinese with English Abstract)
3. Al-Mamoori, A.; Krishnamurthy, A.; Rownaghi, A.A.; Rezaei, F. Carbon capture and utilization update. *Energy Technol.* **2017**, *5*, 834–849. [[CrossRef](#)]
4. Metz, B.; Davidson, O.; Coninck, H.D.; Loos, M.; Meyer, L. *IPCC Special Report on Carbon Dioxide Capture and Storage*; Cambridge University Press: New York, NY, USA, 2005; pp. 51–72.
5. Damen, K.; Faaij, A.; Turkenburg, W. Health, Safety and environmental risks of underground CO<sub>2</sub> storage—Overview of mechanisms and current knowledge. *Clim. Chang.* **2006**, *74*, 289–318. [[CrossRef](#)]
6. Zhao, Y.; Rui, Z.H.; Zhang, Z.; Chen, S.W.; Yang, R.F.; Du, K.; Dindoruk, B.; Yang, T.; Stenby, E.H.; Wilson, M.A. Importance of conformance control in reinforcing synergy of CO<sub>2</sub> EOR and sequestration. *Petrol. Sci.* **2022**, *19*, 3088–3106. [[CrossRef](#)]
7. Ajayi, T.; Gomes, J.S.; Bera, A. A review of CO<sub>2</sub> storage in geological formations emphasizing modeling, monitoring and capacity estimation approaches. *Petrol. Sci.* **2019**, *16*, 1028–1063. [[CrossRef](#)]
8. Hameli, F.A.; Belhaj, H.; Dhuhoori, M.A. CO<sub>2</sub> sequestration overview in geological formations: Trapping mechanisms matrix assessment. *Energies* **2022**, *15*, 7805. [[CrossRef](#)]
9. Khan, S.; Al-Shuhail, A.A.; Khulief, Y.A. Numerical modeling of the geomechanical behavior of Ghawar Arab-D carbonate petroleum reservoir undergoing CO<sub>2</sub> injection. *Environ. Earth Sci.* **2016**, *75*, 1499. [[CrossRef](#)]
10. Newell, P.; Ilgen, A.G. *Overview of Geological Carbon Storage (GCS)*; Report No. SAND2018-3352B662875; Sandia National Lab: Albuquerque, NM, USA, 2018.
11. Khan, S.; Khulief, Y.A.; Al-Shuhail, A.A. Numerical modeling of the geomechanical behavior of Biyadh reservoir undergoing CO<sub>2</sub> injection. *Int. J. Geomech.* **2017**, *17*, 04017039. [[CrossRef](#)]
12. Zhang, L. *Saline Aquifer Storage of CO<sub>2</sub> from Natural Gas Reservoirs in the South China Sea: Trapping Mechanisms and Project Design*; China University of Petroleum (East China): Qingdao, China, 2011. (In Chinese with English Abstract)
13. Zhang, L.; Wen, R.; Geng, S.; Shi, X.; Hao, Y.; Ren, S. Research progress and key issues of CO<sub>2</sub> sequestration in basalt minerals. *J. Chem. Eng. Chin. Univ.* **2022**, *36*, 473–480. (In Chinese with English Abstract)
14. Zhang, L.; Wen, R.; Li, F.; Li, C.; Sun, Y. Assessment of CO<sub>2</sub> mineral storage potential in the terrestrial basalts of China. *Fuel* **2023**, *037*, 157–172. [[CrossRef](#)]
15. Matter, J.M.; Stute, M.; Snæbjornsdottir, S.O.; Oelkers, E.H.; Gislason, S.R.; Aradottir, E.S.; Sigfusson, B.; Gunnarsson, I.; Sigurdardottir, H.; Gunnlaugsson, E.; et al. Rapid carbon mineralization for permanent disposal of anthropogenic carbon dioxide emissions. *Science* **2016**, *352*, 1312–1314. [[CrossRef](#)]
16. McGrail, B.P.; Schaef, H.T.; Ho, A.M.; Chien, Y.J.; Dooley, J.J.; Davidson, C.L. Potential for carbon dioxide sequestration in flood basalts. *J. Geophys. Res.* **2006**, *111*, B12201. [[CrossRef](#)]
17. Zou, C.N.; Zhao, W.Z.; Jia, C.Z.; Zhu, R.K.; Zhang, G.Y.; Zhao, X.; Yuan, X.J. Formation and distribution of volcanic hydrocarbon reservoirs in sedimentary basins of China. *Petrol. Explor. Dev.* **2008**, *35*, 257–271, (In Chinese with English abstract). [[CrossRef](#)]
18. Ren, S.R.; Zhang, L.; Zhang, L. Geological storage of CO<sub>2</sub>: Overseas demonstration projects and its implications to China. *J. Chin. Univ. Petrol.* **2010**, *34*, 93–98. (In Chinese with English Abstract)
19. Liu, Z.; Zhang, N.; Zhang, F. A review on CO<sub>2</sub> geological storage technologies and chemical behaviors of isotope in salty water layer. *Sci. Technol. Rev.* **2015**, *33*, 108–113.
20. Osman, A.I.; Hefny, M.; Abdel Maksoud, M.I.A.; Elgarahy, A.M.; Rooney, D.W. Recent advances in carbon capture storage and utilisation technologies: A review. *Environ. Chem. Lett.* **2021**, *19*, 797–849. [[CrossRef](#)]
21. Bachu, S.; Adams, J.J. Sequestration of CO<sub>2</sub> in geological media in response to climate change: Capacity of deep saline aquifers to sequester CO<sub>2</sub> in solution. *Energ. Convers. Manag.* **2003**, *44*, 3151–3175. [[CrossRef](#)]
22. Czernichowski-Lauriol, I.; Rochelle, C.A.; Brosse, E.; Springer, N.; Bateman, K.; Kervevan, C.; Pearce, J.M.; Sanjuan, B.; Serra, H. Reactivity of Injected CO<sub>2</sub> with the Usira Sand Reservoir at Sleipner, Northern North Sea. In Proceedings of the 6th International Conference on Greenhouse Gas Control Technologies, Kyoto, Japan, 1–4 October 2002; pp. 1617–1620.
23. Gaus, I.; Azaroual, M.; Czernichowski-Lauriol, I. Reactive transport modelling of the impact of CO<sub>2</sub> injection on the clayey cap rock at Sleipner (North Sea). *Chem. Geol.* **2005**, *217*, 319–337. [[CrossRef](#)]
24. Maldal, T.; Tappel, I.M. CO<sub>2</sub> underground storage for Snøhvit gas field development. *Energy* **2004**, *29*, 1403–1411. [[CrossRef](#)]
25. Tenthorey, E.; Boreham, C.J.; Hortle, A.L.; Underschlutz, J.R.; Golding, S.D. Importance of mineral sequestration during CO<sub>2</sub> gas migration: A case study from the Greater Gorgon area. *Energy Procedia* **2011**, *4*, 5074–5078. [[CrossRef](#)]
26. Ma, X.; Li, X.F.; Wen, D.G.; Luo, X.W.; Diao, Y.J.; Yang, G.D.; Yin, S.G.; Cao, W. A study of the potential of field-scale of CO<sub>2</sub> geological storage and enhanced water recovery in the eastern Junggar area of Xinjiang. *Hydrogeol. Eng. Geol.* **2021**, *48*, 196–205. (In Chinese with English Abstract)

27. Gan, M.G.; Nguyen, M.C.; Zhang, L.W.; Wei, N.; Li, J.; Lei, H.W.; Wang, Y.; Li, X.C.; Stauffer, P.H. Impact of reservoir parameters and wellbore permeability uncertainties on CO<sub>2</sub> and brine leakage potential at the Shenhua CO<sub>2</sub> Storage Site, China. *Int. J. Greenh. Gas Control* **2021**, *111*, 103443. [[CrossRef](#)]
28. He, J.; Yao, Y.; Yu, J.; Zhang, J. Petroleum geological characteristics and exploration and development progress of offshore basins in China. *Mar. Geol. Frontier* **2022**, *38*, 1–17. (In Chinese with English Abstract)
29. Wang, J.Q.; Yuan, Y.; Chen, J.W.; Zhang, W.; Zhang, J.; Liang, J.; Zhang, Y.G. Geological conditions and suitability evaluation for CO<sub>2</sub> geological storage in deep saline aquifers of the Beibu Gulf Basin (South China). *Energies* **2023**, *16*, 2360. [[CrossRef](#)]
30. Su, L.; Zheng, J.J.; Chen, G.J.; Zhang, G.C.; Guo, J.M.; Xu, Y.C. The upper limit of maturity of natural gas generation and its implication for the Yacheng formation in the Qiongdongnan Basin, China. *J. Asian Earth Sci.* **2012**, *54–55*, 203–213. [[CrossRef](#)]
31. Al-Khdheawi, E.A.; Mahdi, D.S.; Ali, M.; Fauziah, C.A.; Barifcani, A. Impact of caprock type on geochemical reactivity and mineral trapping efficiency of CO<sub>2</sub>. In Proceedings of the Offshore Technology Conference Asia, Kuala Lumpur, Malaysia, 27 October 2020.
32. Li, Y.; Tian, H.L.; Zhuo, Z.; Sun, Y. The potential effect of CO<sub>2</sub>-water-rock reaction on the caprock formation (mudstone) case study. *Adv. Mater. Res.* **2012**, *518–523*, 140–143. [[CrossRef](#)]
33. Liu, F.Y.; Lu, P.; Griffith, C.; Hedges, S.W.; Soong, Y.; Hellevang, H.; Zhu, C. CO<sub>2</sub>-brine-caprock interaction: Reactivity experiments on Eau Claire shale and a review of relevant literature. *Int. J. Greenh. Gas Control* **2012**, *7*, 153–167. [[CrossRef](#)]
34. Gaus, I. Role and impact of CO<sub>2</sub>-rock interactions during CO<sub>2</sub> storage in sedimentary rocks. *Int. J. Greenh. Gas Control* **2010**, *4*, 73–89. [[CrossRef](#)]
35. Pearce, J.; Underschultz, J.; Croix, A.L. *Mineralogy, Geochemical CO<sub>2</sub>-Water-Rock Reactions and Associated Characterization*; The University of Queensland: Brisbane, Australia, 2019.
36. Soong, Y.; Crandall, D.; Howard, B.H.; Haljasmaa, I.; Dalton, L.E.; Zhang, L.W.; Lin, R.H.; Dilmore, R.M.; Zhang, W.; Shi, F.; et al. Permeability and mineral composition evolution of primary seal and reservoir rocks in geologic carbon storage conditions. *Environ. Eng. Sci.* **2018**, *35*, 391–400. [[CrossRef](#)]
37. Li, J.; Chen, Z.Y.; Feng, Y.C.; Qu, L.S.; Liu, J.G.; Li, W.Y.; Dai, M.Y. Damage of reservoir rock induced by CO<sub>2</sub> injection. *Petrol. Sci.* **2022**, *19*, 1674–1681. [[CrossRef](#)]
38. Gysi, A.P.; Stefánsson, A. Experiments and geochemical modeling of CO<sub>2</sub> sequestration during hydrothermal basalt alteration. *Chem. Geol.* **2012**, *306–307*, 10–28. [[CrossRef](#)]
39. Pearce, J.K.; Brink, F.; Dawson, G.W.; Poitras, J.; Southam, G.; Paterson, D.J.; Wolhuter, A.; Underschultz, J.R. Core characterisation and predicted CO<sub>2</sub> reactivity of sandstones and mudstones from an Australian oil field. *Int. J. Coal Geol.* **2022**, *250*, 103911. [[CrossRef](#)]
40. Liu, H.; Ren, Y.L.; Li, X.; Hu, Y.X.; Wu, J.P.; Li, B.; Luo, L.; Tao, Z.; Liu, X.; Liang, J.; et al. Rock thin-section analysis and identification based on artificial intelligent technique. *Petrol. Sci.* **2022**, *19*, 1605–1621. [[CrossRef](#)]
41. Ma, H.; Han, G.Q.; Peng, L.; Zhu, L.Y.; Shu, J. Rock thin sections identification based on improved squeeze-and-Excitation Networks model. *Comput. Geosci.* **2021**, *152*, 104780. [[CrossRef](#)]
42. Apps, J.A.; Zheng, L.; Spycher, N.; Birkholzer, J.T.; Kharaka, Y.; Thordsen, J.; Kakouros, E.; Trautz, R. Transient changes in shallow groundwater chemistry during the MSU-ZERT CO<sub>2</sub> injection experiment. *Energy Procedia* **2011**, *4*, 3231–3238. [[CrossRef](#)]
43. CMG. *GEM Manual v2021.10*; Computer Modelling Group Ltd.: Calgary, AB, Canada, 2021.
44. Nghiem, L.; Sammon, P.; Grabenstetter, J.; Ohkuma, H. Modeling CO<sub>2</sub> Storage in Aquifers with a Fully-Coupled Geochemical EOS Compositional Simulator. In Proceedings of the SPE-89474, SPE/DOE Symposium on Improved Oil Recovery, Tulsa, OK, USA, 17 April 2004.
45. Ji, L.; Zhang, T.; Milliken, K.; Qu, J.; Zhang, X. Experimental investigation of main controls to methane adsorption in clay-rich rocks. *Appl. Geochem.* **2012**, *27*, 2533–2545. [[CrossRef](#)]
46. Garcia, J.E. *Fluid Dynamics of Carbon Dioxide Disposal into Saline Aquifers*. University of California: Berkeley, CA, USA, 2003.
47. Wu, D.S. *Fundamentals of Chemical Engineering*; Higher Education Press: Beijing, China, 2000; Volume 1. (In Chinese)
48. Cui, G.D.; Zhu, L.H.; Zhou, Q.C.; Ren, S.R.; Wang, J.Y. Geochemical reactions and their effect on CO<sub>2</sub> storage efficiency during the whole process of CO<sub>2</sub> EOR and subsequent storage. *Int. J. Greenh. Gas Control* **2021**, *108*, 103335. [[CrossRef](#)]
49. Alemu, B.L.; Aagaard, P.; Munz, I.A.; Skurtveit, E. Caprock interaction with CO<sub>2</sub>: A laboratory study of reactivity of shale with supercritical CO<sub>2</sub> and brine. *Appl. Geochem.* **2011**, *26*, 1975–1989. [[CrossRef](#)]
50. Wollenweber, J.; Alles, S.; Busch, A.; Krooss, B.M.; Stanjek, H.; Littke, R. Experimental investigation of the CO<sub>2</sub> sealing efficiency of caprocks. *Int. J. Greenh. Gas Control* **2010**, *4*, 231–241. [[CrossRef](#)]
51. Gherardi, F.; Xu, T.; Pruess, K. Numerical modeling of self-limiting and self-enhancing caprock alteration induced by CO<sub>2</sub> storage in a depleted gas reservoir. *Chem. Geol.* **2007**, *244*, 103–129. [[CrossRef](#)]
52. Luquot, L.; Gouze, P. Experimental determination of porosity and permeability changes induced by injection of CO<sub>2</sub> into carbonate rocks. *Chem. Geol.* **2009**, *265*, 148–159. [[CrossRef](#)]
53. Kim, K.; Vilarrasa, V.; Makhnenko, R.Y. CO<sub>2</sub> injection effect on geomechanical and flow properties of calcite-rich reservoirs. *Fluids* **2018**, *3*, 66. [[CrossRef](#)]

54. Yang, G.; Ma, X.; Feng, T.; Yu, Y.; Yin, S.; Huang, M.; Wang, Y. Geochemical modelling of the evolution of caprock sealing capacity at the Shenhua CCS Demonstration Project. *Minerals* **2020**, *10*, 1009. [[CrossRef](#)]
55. Huo, C.L. *Study on Potential Evaluation and the Storage Areas of the Carbon Dioxide Seabed Storage in Offshore China*; Dalian Maritime University: Dalian, China, 2014.

**Disclaimer/Publisher's Note:** The statements, opinions and data contained in all publications are solely those of the individual author(s) and contributor(s) and not of MDPI and/or the editor(s). MDPI and/or the editor(s) disclaim responsibility for any injury to people or property resulting from any ideas, methods, instructions or products referred to in the content.